WATER RESOURCES RESEARCH, VOL. 31, NO. 12, PAGES 3205–3215, DECEMBER 1995 1995

Episodic and constant flow models for the origin of low-chloride waters in a modern accretionary complex

Barbara A. Bekins,[1] Anne M. McCaffrey, and Shirley J. Dreiss[2]
Earth Sciences Department, University of California, Santa Cruz

Abstract. Some low-chloride pore waters observed in accretionary complexes are thought to result from clay dehydration and subsequent migration of the released water along faults or sand layers. We test this hypothesis with a two-dimensional flow and transport model for a cross section of the northern Barbados accretionary complex. The model flow system is driven by consolidation of the accreted sediments and by fluids from smectite clay dehydration. Steady state simulations result in concentrations that are too high along the décollement fault and too low near the seafloor. In a transient model we simulate buildup and release of fluids by assuming that strain or hydrofracture along the fault causes an instantaneous increase in décollement permeability of 2–3 orders of magnitude. With such an increase, the observed concentrations can be achieved in 100–1000 years. Also pressures along the fault rise to near lithostatic values in 10–100 years and remain high for 1000–10,000 years. This pressure rise may represent a mechanism for sustaining high fault permeabilities long after the initial increase.

Introduction

Appreciation for the role of porous media flow in submarine environments is growing rapidly. The discovery of black smokers and the convection cells driving them was followed more recently by evidence for vigorous flow along active plate margins. The most dramatic evidence for such flow consists of fluid vents on the seafloor that support communities of exotic benthic organisms [*Suess et al.*, 1985; *Kulm et al.*, 1986]. The vents are found near the toes of sedimentary accretion-subduction complexes which form in subduction zones when seafloor sediments on the subducted plate are scraped off or underplated at the edge of the upper plate. The detachment surface separating the sediments accreted to the upper plate from those subducted with the downgoing plate is called the décollement. Although the accretion process starts deep in an ocean trench, many complexes grow until eventually they rise above sea level and form mountain belts such as the Oregon and Washington Coast Ranges. The Barbados Ridge complex, shown in Figure 1, is growing at the edge of the Caribbean plate from sediments scraped off the downgoing Atlantic plate. It is subaerially exposed only at Barbados Island. This complex represents an end-member in a classification of sedimentary accretionary complexes because it is composed of low-permeability clays and silts and is growing very slowly.

A steady source of pore fluids enters an accretionary complex with the accreted seafloor sediments. These fluids may then affect a variety of geologic processes. For example, high pore pressures affect fault strength and seismicity [*Magee and Zoback*, 1993], and fluid-rock interactions influence metamorphic reactions [*Peacock*, 1990]. In a thorough review of fluid flow in accretionary prisms, *Moore and Vrolijk* [1992] described two processes that drive the flow system. One is the very high mechanical loading rate on the saturated sediments as they are either incorporated into or underthrust below the complex. This loading rate is up to 15 times the maximum due to sedimentary basin subsidence [*Moore and Vrolijk*, 1992; *Neuzil*, 1995]. The resulting consolidation is often limited by low permeabilities, leading to near-lithostatic pore pressures. A second process is the dehydration of minerals and generation of hydrocarbons as sediments buried deep in the complex are subjected to higher temperatures. Anomalously low chloride and high methane concentrations in pore waters suggest that this is occurring in many accretionary complexes [*Kastner et al.*, 1991]. The elevated temperatures and exotic chemical signatures of the pore fluids indicate that the flow systems supplying the vents may extend, in some cases, for 50–100 km. However, the source of heat and solutes is still poorly understood. Figure 1c shows pore water chloride and methane concentration changes with depth at Ocean Drilling Program (ODP) site 671 in the Barbados Ridge complex. The pore waters are almost 10% lower in chloride than seawater at the depth of the décollement fault. In addition, more recent chloride concentrations from the décollement at ODP site 948 (near site 671) were 20% lower than that of seawater [*Kastner et al.*, 1994].

Gieskes et al. [1990] discussed clay membrane filtration, hydrate dissolution, and the dehydration of smectite clay as possible sources for the low-chloride water. They argued against the first two on the basis of oxygen isotope data and the scarcity of hydrates in the area and favored the clay dehydration hypothesis. Smectite commonly occurs in random interlayers with illite such that the combined mineral is know as illite/smectite (I/S). At temperatures above 60°C, the percent of smectite in I/S begins to decrease, as smectite layers react with potassium and aluminum to form illite plus water and silica. The water released in the reaction is 20% by weight. The conversion results in a porosity increase as solid components of smectite are replaced by unbound fluid plus illite. If the porous frame-

[1]Now at U.S. Geological Survey, Menlo Park, California.
[2]Deceased December 14, 1993.

Paper number 95WR02569.
0043-1397/95/95WR-02569$05.00

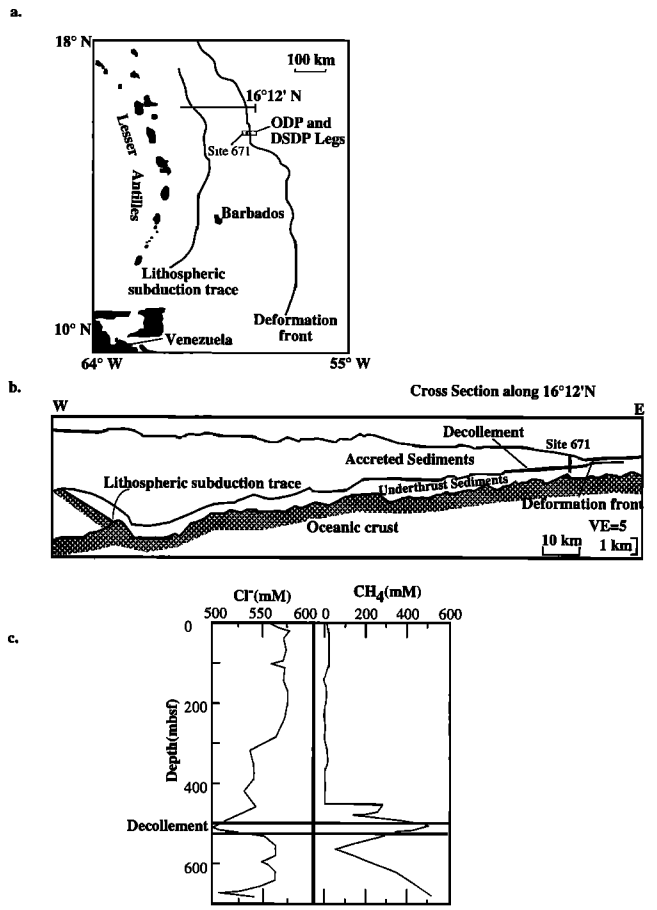

Figure 1. (a) Map of the eastern Caribbean showing the deformation front (the first sign of deformation on the seafloor where the Atlantic plate is subducted beneath the Caribbean plate) and lithospheric subduction trace (where the lithosphere of the subducted plate passes below that of the upper plate). Ocean Drilling Program (ODP) leg 110, site 671 is shown along with the location of the first full seismic image of an accretionary complex at 16°12′ [*Westbrook et al.*, 1988]. (b) Cross section of the Barbados Ridge accretionary complex along 16°12′ based on data from *Westbrook et al.* [1988]. The complex consists of a 6- to 7-km-deep by 125-km-wide prism of seafloor sediments scraped off onto the leading edge of the Caribbean plate; a section of approximately 400 m of underthrust sediments carried down with the subducting Atlantic oceanic crust; and a roughly 30-m-thick detachment, called the décollement, separating the two. The location and depth of ODP site 671 are shown. (c) Concentration versus depth of chloride and methane in pore water at ODP site 671. The chloride concentrations along the décollement at 500 m and in a high-permeability sand horizon at 680 m are about 10% lower than seawater. Methane concentrations show an opposite trend, increasing along the same horizons (data from *Gieskes et al.* [1990]). Depth is in units of meters below seafloor (mbsf).

work subsequently collapses, the released fluid will be driven from the reaction zone. The Barbados complex sediments initially contain abundant smectite, but they are not heated sufficiently to release the interlayer water until they are buried to depths of at least 3 km [*Bekins et al.*, 1994]. Owing to the low taper angle of this prism, a 3-km burial depth is not achieved for a distance of at least 50 km from the toe of the complex. Thus, to reach the observation sites, the water produced by the reaction must be transported more than 50 km along the décollement fault zone. The implication is that an extensive regional flow system exists that is dominated by channeled flow along faults.

Recently, several workers have measured permeabilities of accretionary complex sediments both in the laboratory and in the field. The laboratory data indicate that permeabilities of clay-rich sediments drop as they are sheared in a fault zone [*Brown et al.*, 1994]. However, field slug tests [*Screaton et al.*, 1995; *Fisher and Zwart*, 1994] and laboratory data [*Brown*, 1995] indicate that the log of permeability is a linear function of effective stress. Because the chemical data from the field indicate that flow is channeled along the faults, the implication is that relatively high permeability is maintained in the fault zones by high fluid pressures. This picture is supported by seismic data that show reversed polarity reflectors along the known fault planes. The reversed polarity signal indicates a transition to lower velocity and/or density sediments and has been interpreted as a dilated fault zone [*Bangs and Westbrook*, 1991]. The emerging picture is that fluids are transported along fault zones which are dilated in pockets of limited spatial dimensions [*Bangs and Westbrook*, 1991; *Shipley et al.*, 1994].

The purpose of this work is to test whether physically feasible flow and transport scenarios incorporating the water released by smectite dehydration can cause the observed chloride anomalies at Barbados. If the results are positive, it should be possible to generalize them to other modern complexes worldwide. To accomplish this goal, a flow and transport model was constructed for a vertical cross section at the latitude of the ODP leg 110 transect of the Barbados complex. The model is similar in its conceptualization to that of *Screaton et al.* [1990], who modeled fluid flow in a 20-km-long cross section of the toe of the Barbados complex. The model described here, however, encompasses the entire accretionary complex and includes the zone of smectite dehydration. Within this model domain, fluids are produced solely from sediment compaction and smectite dehydration. Because the oceanic basement and arcward boundary are relatively impermeable, these fluids must leave the model domain across the seafloor boundary or out the toe of the complex. The model results constrain the décollement permeability that is required to produce the observed chloride concentrations and pore pressures. Both the permeability and the persistence of dilated fractures are examined.

Model Description

In the northern part of the Barbados complex along the ODP leg 110 transect, the clay-rich, hemipelagic sediment sequence on the Atlantic plate is presently about 700 m thick with one third of this being accreted (Figure 1b) [*Moore and Biju-Duval*, 1984]. Estimates for the total age of the prism vary from late Eocene (40 m.y.) [*Speed and Larue*, 1982] to Late Cretaceous (60 m.y.) [*Bouysse et al.*, 1990]. Measured values of average bulk illite/smectite in this section vary from 40 to 72%, and within the I/S, 78–100% of the interlayers are smectite [*Tribble*, 1990; *Capet et al.*, 1990]. Thus the bulk smectite containing interlayer water ranges from 32% to 72% by weight. Sediments in the toe of the prism are predominantly calcareous clays and mudstones with thin ash layers [*Moore et al.*, 1988]. The décollement was first described from drill core observations as an approximately 30-m section of intensely deformed scaley fabrics [*Moore and Biju-Duval*, 1984]. How-

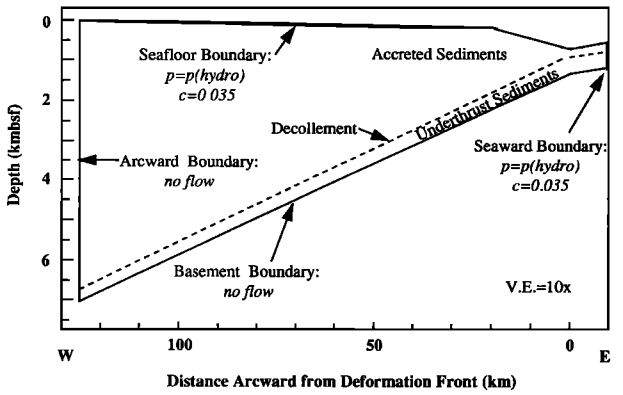

Figure 2. Sketch of the model geometry and boundary conditions. At the deformation front an incoming sediment thickness of 620 m is divided into a 230-m accreted section and a 390-m underthrust sequence separated by a 30-m décollement. Seaward of 20 km the taper angle of the wedge is 3.2°, and arcward of this the taper angle is 2.8°. The oceanic basement and arcward boundaries are assumed to be no flow, while the seafloor and seaward boundaries are held at hydrostatic pressure with the concentration set to the total dissolved solids in seawater.

ever, *Shipley et al.* [1994] suggested, on the basis of synthetic seismic models of the décollement, that the pressurized sections imaged as reversed polarity reflections are no more than 14 m thick. A recent series of single borehole pulse and constant flow tests performed on ODP leg 146 [*Screaton et al.*, 1995] indicate that permeability along an accretionary prism fault ranged from 10^{-15} m^2 to 10^{-11} m^2. In addition, packer tests performed near site 671 on ODP leg 156 measured décollement permeabilities from 10^{-15} m^2 to greater than 10^{-13} m^2 [*Fisher and Zwart*, 1994].

The cross-section model consists of three zones: the accretionary prism; the décollement fault zone; and the underthrust sediments (Figure 2). Physical properties for each zone are estimated on the basis of geological observations. The model domain is divided into a finite element grid consisting of 24,056 nodes and 23,250 quadrilateral elements. The large-scale geometry follows the interpreted seismic profile shown in Figure 1b [*Westbrook et al.*, 1988], whereas geometry near the toe follows that observed during ODP leg 110. Horizontally, the model extends from 10 km seaward of the deformation front to 125 km arcward, encompassing the entire complex at this latitude. The wedge taper angle is 3.2° for the first 20 km near the toe and then decreases to 2.8° for the remainder of the complex. The total sediment thickness is 620 m at the toe and thickens gradually to about 7 km at the arcward end. At the deformation front the incoming sediment sequence is divided into 390 m of underthrust sediments and 230 m of accreted sediments. Between the two, a 30-m décollement zone is made up of 15 m from each section.

The choice of reference frame for the model exploits the fact that accretionary complexes maintain a self-similar shape as they grow. *Davis et al.* [1983] showed this by conceiving of a growing wedge as a pile of cohesionless sediment in front of a hypothetical bulldozer. The shape of such a wedge is constant over time and depends only on the strength of the sediments and the friction on the base. By pinning the model reference frame to the tip or deformation front of the growing wedge, it is possible to avoid having the model size change with time. The sediments move through the self-similar shape by being accreted to the toe and then buried in the complex as new sediments are added to the front. In this reference frame, sediments enter the complex with a relative velocity equal to sum of the plate convergence rate and the advance rate of the deformation front. At this latitude, *Le Pichon et al.* [1990] suggested using an initial relative velocity of 21 mm/yr. Although this approach is not adequate for tracking the entire history of the complex, it gives a reasonable estimate of the fluid sources driving the present flow system. However, it is important to limit the length of the simulations to account for the age of the prism at site 671. Assuming a relative convergence rate of 21 km/m.y. and accounting for a 30% slowing as the prism thickens, the sediments at site 671 were probably accreted about 0.2 Ma. Thus the simulations should be limited to less than 0.1 m.y.

To describe the fluid flow a two-dimensional, variable density, transient flow equation is used:

$$(\rho S_{op})\frac{\partial p}{\partial t} + \left(\varepsilon\frac{\partial \rho}{\partial C}\right)\frac{\partial C}{\partial t} - \nabla\cdot\left[\left(\frac{\mathsf{k}\rho}{\mu}\right)\cdot(\nabla p - \rho g)\right] = Q_p \tag{1}$$

where p is pressure ($ML^{-1}T^{-2}$), ρ is fluid density (ML^{-3}), S_{op} is specific pressure storativity (LT^2M^{-1}), ε is porosity (dimensionless), C is concentration of total dissolved solids (dimensionless), k is the permeability tensor (L^2), μ is viscosity ($ML^{-1}T^{-1}$), and Q_p ($ML^{-3}T^{-1}$) accounts for the fluids produced by compaction and dehydration. The specific pressure storativity is defined by $S_{op} = (1 - \varepsilon)\alpha + \varepsilon\beta$ where α (LT^2M^{-1}) and β (LT^2M^{-1}) are the porous matrix and fluid compressibilities, respectively. Thermal expansion is neglected because it changes the normalized pressures by less than 1%.

To describe the transport of total dissolved solids, the two-dimensional advective-dispersive equation is used:

$$\varepsilon\rho\frac{\partial C}{\partial t} + \varepsilon\rho\mathbf{v}\cdot\nabla C - \nabla\cdot[\varepsilon\rho(D_m\mathsf{I} + \mathsf{D})\cdot\nabla C] = Q_p(C^* - C) \tag{2}$$

where $\mathbf{v} = \mathbf{v}_s + \mathbf{v}_w$, $\mathbf{v}_s$ is the sediment velocity vector (LT^{-1}), $\mathbf{v}_w$ is the fluid average linear velocity relative to the sediments (LT^{-1}), D_m is molecular diffusivity (L^2T^{-1}), I is the identity matrix, D is the dispersion tensor relative to the sediments (L^2T^{-1}), and C^* is the concentration of total dissolved solids in the source fluid (dimensionless).

Two modifications of the computer code SUTRA [*Voss*, 1984] were made before using it to solve the above equations. The first allows specification of sediment temperatures and uses them to compute fluid viscosities according to the relation given by *Voss* [1984]. The second modification allows estimated sediment velocities to be specified and uses them to convert relative fluid flow velocities (computed relative to the moving sediments) to absolute flow velocities. This conversion is discussed in detail by *Screaton et al.* [1990]. It is necessary because the sediments move through the model reference frame carrying pore water with them. Simultaneously, pressure-driven flow occurs, and Darcy's law gives the resulting velocity relative to the moving sediments. Velocities that appear in the transport equation must incorporate both the transport due to motion of the sediments and the relative fluid flow driven by pressure gradients. Thus the vector sum of the sediment ve-

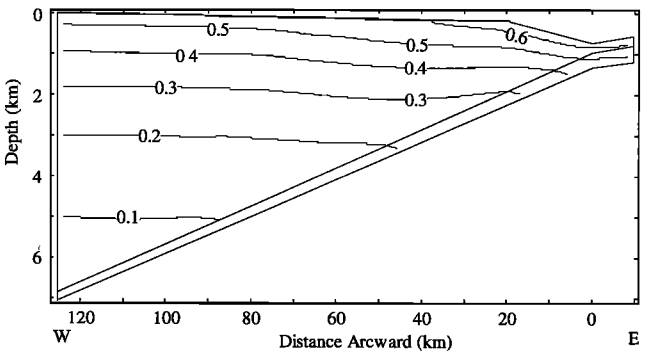

Figure 3. Contour plot of estimated porosities in the complex. The values roughly correspond to those determined by *Bangs et al.* [1990] from seismic velocities.

locities and the relative pressure–driven fluid velocities is termed the absolute fluid velocity. This absolute velocity, $\mathbf{v} = \mathbf{v}_s + \mathbf{v}_w$, is used for the advective term in (2), while the relative velocity, $\mathbf{v}_w$, is used to compute the mechanical dispersion tensor, D, using the formula of *Voss* [1984].

The boundary conditions for the flow and transport model are shown in Figure 2. At the east side or seaward end of the complex, hydrostatic pressures for seawater are specified. Similarly, the seafloor boundary is hydrostatic. Along the base of the complex, the oceanic crust is treated as a no-flow boundary ($\mathbf{v}_w = 0$). This assumption is based on the supposition that most fractures are filled in the 82 m.y. old crust. At the west side, or arcward end of the complex, the permeabilities and the fluid sources from compaction and dehydration are very low. The fluid crossing this boundary will primarily be transported by the moving sediments rather than by pressure-driven flow. Therefore the boundary is also treated as no flow ($\mathbf{v}_w = 0$). Fluid enters the complex at the seaward vertical boundary carried in the pores of the moving sediments. The concentration of this fluid is assumed to be equivalent to the total dissolved solids in seawater, or 35,000 parts per million.

Two types of simulations are performed: steady state and transient. In the steady state simulations the assumption is that fluid must exit the complex at the same rate that it is produced. Thus the pressures and concentrations depend only on position in the complex, and the time derivatives in (1) and (2) vanish. In the transient simulations the full equations (1) and (2) are solved. The hypothesis is that pressures in the complex build until they reach values close to lithostatic levels. The high pressures lower the effective stress along the décollement fault, permitting a strain event to occur. The strain, in turn, creates fractures or dilates existing fractures, raising the permeability along the fault. To simulate this scenario, a series of steady state runs are made with varying values of décollement permeability (k_d). The k_d that leads to slightly sublithostatic fluid pressure is determined. We then assume that the pressures and concentrations from this solution represent those in the complex just before a slip event that increases k_d and use these values as initial conditions in the transient simulations. In all transient simulations the aquifer compressibility is 10^{-7} Pa^{-1}, which is suitable for clay. The values used for $\partial\rho/\partial C$ and β are those given by *Voss* [1984].

Because the entire flow system is driven by the fluid sources within the model domain, reliable estimates of these sources are crucial. The pore fluids lost by compaction can be computed by performing a mass balance on a sediment packet as it moves through the complex. Figure 3 shows the idealized model porosity distribution based on values inferred by *Bangs et al.* [1990] from seismic data. The rate of fluid production for sediments moving through a fixed porosity distribution is given by the divergence of the sediment velocity field [*Screaton et al.*, 1990]. *Bekins and Dreiss* [1992] used a kinematic model of the prism with uniformly divergent sediment trajectories to find an analytic solution for the sediment velocities:

$$v_{s_x} = v_{0_x} \frac{(1-\varepsilon_0)}{(1-\varepsilon)} \frac{z_0}{z} \qquad v_{s_y} = v_{s_x} \frac{v_{0_y}}{v_{0_x}} \tag{3}$$

where v_{0_x}, v_{0_y}, ε_0, and z_0 are the horizontal and vertical velocity, porosity, and depth of sediments entering the complex, and v_{s_x}, v_{s_y}, ε, and z are the horizontal and vertical velocity, porosity, and depth of sediments at the current position in the complex. Substituting values for the geometry, porosities, and initial velocity into (3) provides sediment velocity estimates and the rate of compaction dewatering in the complex. Figure 4a is a contour plot of the log of the fluid production rate in cubic meters of fluid per cubic meters of sediment per second. (These source values must be multiplied by the fluid density to obtain Q_p in (1).) The results indicate that compaction fluid sources are highest at the toe of the complex

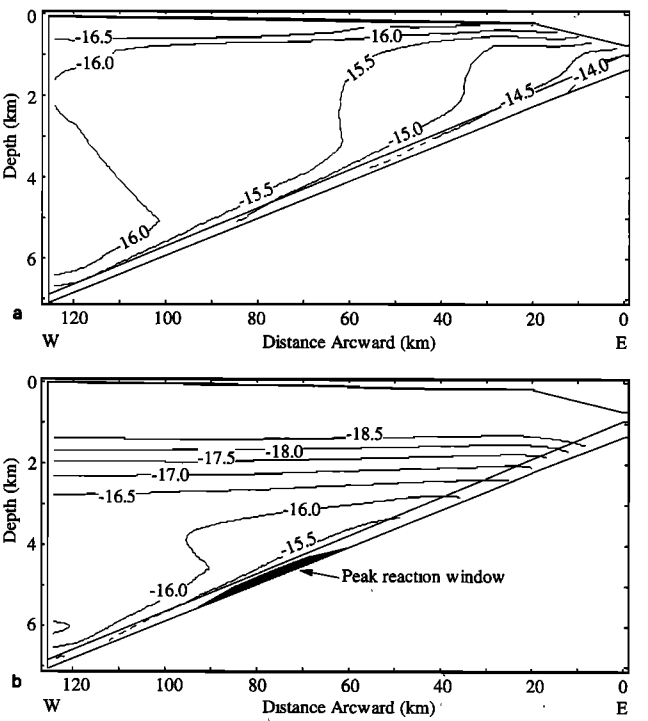

Figure 4. (a) Contour plot showing the rate at which pore fluid is squeezed by compaction from sediments in the complex as they are subjected to increased burial. The units are log of fluid volume per unit sediment volume per second. The maximum values are found near the deformation front and in the underthrust section where the rate of loading is highest. (b) Contour plot of the rate that fluid is released by smectite dehydration assuming a bulk smectite content of 40%. The peak reaction rate in the underthrust is between 60 and 90 km and corresponds to 10^{-15} s^{-1}. The rate in the underthrust sediments is faster because the temperatures are higher and because the subducting sediments pass through the reaction window 5 times faster than in the prism.

where they exceed 10^{-14} s^{-1}. They rapidly drop an order of magnitude in the prism by about 40 km arcward. However, in the underthrust sequence, the values remain greater than 10^{-15} s^{-1} until about 90 km arcward. These results can be compared to estimates compiled by *Neuzil* [1995] for a variety of geologic settings. The values near the toe of the complex are similar to those obtained by *Screaton et al.* [1990] in a smaller model of this same cross section, and are roughly the maximum Neuzil found for any setting. The values in the underthrust beyond 60 km are comparable to Gulf Coast compaction estimates obtained by *Bethke* [1986].

Deep in the complex, where compaction sources are relatively insignificant, clay dehydration is the main fluid source. To obtain the rate of smectite dehydration, *Bekins et al.* [1994] applied an existing reaction kinetics model with a temperature dependent rate constant. Temperatures in the complex increase with depth but are perturbed by the prism growth and rapid underthrusting of colder sediments and oceanic crust. To estimate the temperatures, a one-dimensional conductive heat flow model developed by *Ferguson et al.* [1993] was used. The results predict that peak temperatures at the base of the complex exceed 120°C. Because this is near the upper limit of the reaction, the predicted zone of smectite dehydration is almost entirely located within the complex [*Bekins et al.*, 1994]. The effect of advective heat transport has been neglected because it raises temperatures in the bulk sediments by only a few degrees and thus has a minor effect on the clay transformation. Increases of as much as 20°C are concentrated along faults [*Vrolijk et al.*, 1991], but the smectite within the fault zones represents a small proportion of the total.

A fifth-order reaction model [*Pytte and Reynolds*, 1988] for smectite dehydration was selected from among numerous kinetic models in the literature. Although there is no theoretical justification for the use of a fifth-order model, this relation gives the best empirical fit to existing data that span the large range of time-temperature histories experienced by sediments in the prism and underthrust. The kinetic expression is

$$\frac{dX}{dt} = -Ae^{-E/RT}\left(\frac{\mathrm{K}}{\mathrm{Na}}\right)X^5 \qquad (4)$$

where X is the mole fraction of smectite in mixed layer illite/smectite; A is a fitted scale factor of 5.2×10^{-7} s^{-1}, E is the activation energy equal to 33 kcal/mol; R is the gas constant; T is temperature in degrees kelvin, and K/Na is the ratio of activity of K to Na and is equal to $74.2e^{(-2490/T)}$. Figure 4b is a contour plot showing the log of the predicted rate of fluid production from smectite dehydration along the model transect. The rates are higher in the underthrust section than in the prism because of the difference in sediment velocities in the two zones. The underthrust sediments, moving at the subduction velocity, take 4 m.y. to pass through the peak reaction temperature window, whereas the accreted prism sediments take about 20 m.y. The peak fluid production rate reaches about 10^{-15} s^{-1} at the base of the underthrust section between 60 and 90 km arcward. This value is comparable to that obtained by *Bethke* [1986] for smectite dehydration in the Gulf Coast. Although the estimate is based on uniformly diverging sediment trajectories in the prism, the actual sediment motion is probably better described by velocities that are more rapid at the base of the complex. This would result in lower exposure times and more rapid transit through the reaction window. The resulting source terms at the base of the prism would be closer to those shown in Figure 4b for the underthrust sediments. The effect on the concentrations observed in the décollement, however, should be minor, because most of the fluid from the prism leaves the complex along the seafloor and very little flows downward into the décollement.

A difficult aspect of the smectite source computation is accounting for the net volume change during the reaction. Because of expansion of the released water [*Hawkins and Egelstaff*, 1980], the illite plus water should occupy 5% more volume than the original smectite [*Ransom and Helgeson*, 1994]. This minor volume change would produce a relatively minor effect on pore pressures and flow, unless the released water is then subject to removal by collapse of the pore framework. In the underthrust section, porosity estimates of *Bangs et al.* [1990] show a high-porosity anomaly at the center of the peak reaction window (Figure 4b). Their data suggest that the porosity in the underthrust section increases from 10 to 20% as smectite is replaced by illite plus unbound water. Then, as the pore framework collapses in the unlithified sediments, the porosities decrease again to 10%. On the basis of this scenario, the fluid source volume in the underthrust is estimated to be 105% of the values in Figure 4b. In other words, the fluid released by the reaction expands by 5% and is all driven off by subsequent compaction of the pore framework. In contrast, the prism sediments are quite well lithified, and the pore framework may not collapse so readily. Therefore in the prism we include only the expansion of the released water as source terms (or 5% of the values in Figure 4b) and assume that the pore framework does not collapse after the reaction.

Sediment permeabilities are a crucial element of the model. Laboratory permeability measurements of ODP leg 110 samples obtained by *Taylor and Leonard* [1990] show an enormous amount of scatter and only apply to sediments from less than 500 m depth. *Neuzil* [1994] created a composite plot of permeability and porosity data for clays and shales which indicates that a linear relation between log k and porosity is valid for the full range of porosities. Figure 5 shows that the data from ODP sites 671 and 676 mainly fall within the area of Neuzil's compiled data. Thus, to extend the ODP data to depth, we visually placed the line m which roughly bisects the outlined area:

$$\log(k) = -22.0 + 8.44\varepsilon \qquad (5)$$

where k is permeability in square meters and ε is porosity. The contour plot in Figure 6 illustrates the log of permeabilities computed from (5) using the porosities in Figure 3. The values range from about 10^{-16} m^2 near the toe to less than 10^{-21} m^2 at the deepest part. The sensitivity to this distribution is tested by adding ± 0.3 to (5), thus shifting the line m along the log permeability scale (high (h) and low (l) lines are shown with dashes in Figure 5). Permeabilities in the fault are assigned separately in order to simulate the channeling of flow along it. On the basis of the existing data, we perform a series of simulations in which the décollement permeability (k_d) is varied over 10^{-15} m^2 to 10^{-12} m^2. In addition, to check the model, simulations were performed with the same bulk permeability distribution that *Screaton et al.* [1990] used in their smaller model. They used the function formulated by *Morin and Silva* [1984], which is also plotted in Figure 5.

Results and Discussion

Steady State Modeling Results

The permeability distribution was tested by comparing the computed pore pressures to observed and inferred values. To

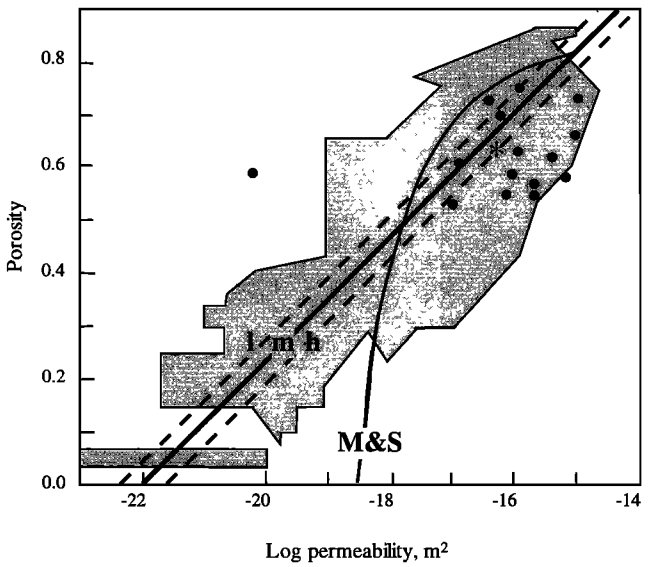

Figure 5. Permeability data measured by *Taylor and Leonard* [1990] for samples from ODP leg 110 (solid circles) superimposed on a large-scale permeability versus porosity outline for argillaceous sediments compiled by *Neuzil* [1994]. The ODP data fall mainly within the boundaries of *Neuzil*'s [1994] plot but there are no ODP data for porosities below 50%. To extend the data to depth, the three porosity-permeability functions denoted l, m, and h were tested with the model. The curve denoted M&S is the function of *Morin and Silva* [1984] that was used by *Screaton et al.* [1990] in a smaller model of the Barbados complex.

Table 1. Summary of Steady State Runs

Run	Permeability: Bulk	Permeability: log (k_d)	Maximum λ*: Value	Maximum λ*: Location, km	Site 671: λ*	Site 671: Concentration
1	h	−13	0.39	118	0.16	537.6
2	h	−14	0.59	17	0.33	550.4
3	h	−15	1.30	58	0.21	560.0
4	l	−13	1.54	123	0.29	532.8
5	l	−14	1.67	17	0.95	540.8
6	l	−15	3.08	58	1.24	558.4
7	m	−13	0.78	122	0.22	534.4
8	m	−14	0.98	16	0.59	544.0
9	m	−15	2.01	58	0.52	560.0
10	m with cap	−13	0.98	0	0.45	532.8
11	m with cap	−14	7.29	0	3.38	542.4
12	h with cap	−13	0.96	0	0.44	534.1
13	h with cap	−14	6.65	0	3.03	549.4
14	M&S	−14	0.83	0	0.55	560.0

Each line lists the bulk permeability distribution and k_d used in the model, together with the computed values for maximum λ* over the whole model, λ* along the décollement at site 671, and the chloride concentration at site 671. See Figure 5 for graph of lines l, m, and h. The label "cap" refers to the addition of a 15-m-thick low-permeability layer above the top of the décollement based on an anomalously low value measured by *Taylor and Leonard* [1990] at site 671. They speculated that the presence of this layer provided a mechanism for maintaining high pore pressures along the décollement. (The sample had a permeability of 6.5×10^{-21} m² and a porosity of 0.58 and falls outside *Neuzil*'s [1994] outline in Figure 5.) The final scenario listed, denoted M&S, refers to the permeability distribution published by *Morin and Silva* [1984] and used in the model of *Screaton et al.* [1990].

compare observations over the wide range of pressures in the model, pore pressures are normalized to lithostatic according to

$$\lambda^* = \frac{P - P_{\text{hydro}}}{P_{\text{litho}} - P_{\text{hydro}}}. \quad (6)$$

where P is pore pressure, P_{hydro} is hydrostatic pressure, and P_{litho} is lithostatic pressure. The value of λ* is zero at hydrostatic pressure and one at lithostatic pressure. Values greater than one cannot be sustained, thus providing one constraint on the model. Another constraint follows from an analysis of the mechanical force balance in an accretionary wedge presented by *Davis et al.* [1983]. Their results indicate that in order for the sediments of the wedge to move over the underthrust sequence along a low-angle décollement, there must be high pore pressures along the entire décollement fault. Lower pressures would result in a steeper taper angle than that observed. The pressure distribution may be patchy in reality, but the average pressure overall must be high. Thus the ideal model results should produce high pore pressures along the entire prism base. A final constraint comes from a recent series of packer tests performed during ODP leg 156 [*Fisher and Zwart*, 1994]. The interval isolated by the packer encompassed the entire décollement zone in ODP hole 948D located near site 671. The pressure at the end of the first pulse test was about 60% of lithostatic. Because the pressures continued to rise over the series of tests, the actual value may be higher. However, on the basis of this test, we constrained the computed λ* near site 671 to be 0.60.

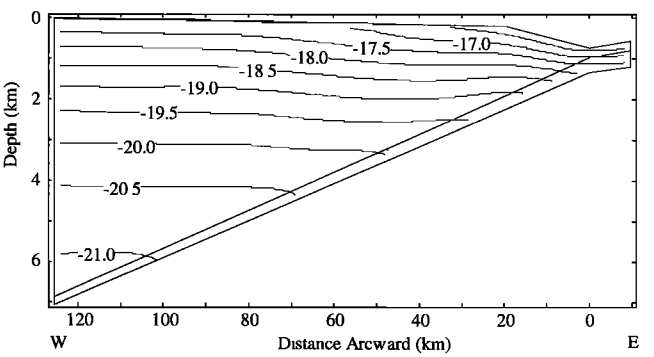

Figure 6. Contour plot of the log of permeability (square meters) computed from the porosities in Figure 3 and the middle (m) porosity-permeability trend in Figure 5.

The results of the steady state runs in Table 1 show that only the permeability distributions numbered 8, 10, 12, and 14 give maximum values of λ* less than one and values at site 671 that are close to 0.60. When the bulk permeabilities were assigned from the lower line (l) in Figure 5, all possible k_d values give maximum λ* values greater than one. In contrast, when bulk permeabilities were assigned from the higher line (h), the values of λ* are all too low to match the site 671 observation. Lines that deviate farther from the line m give results that are even less satisfactory, indicating that the system is quite sensitive to the bulk permeability distribution. With permeabilities assigned from the line m, a k_d of 10^{-14} m² gives the best match to the pressure data. This optimal value for k_d was also obtained by *Screaton et al.* [1990] in their model covering the first 15 km near the toe. The contour plot in Figure 7 shows values of λ* resulting from bulk permeabilities using the line m and a k_d of 10^{-14} m². The high values along the base satisfy the

constraint imposed by *Davis et al.*'s [1983] force balance. We also considered four scenarios in which the permeability cap is added above the décollement. Of these, both 10 and 12 are reasonable, although the results are not as close to the measured pressure at 671 as those from 8.

Examination of Figure 5 shows that most of *Taylor and Leonard*'s [1990] measured sample permeabilities are higher than line m. However, several of the data values fall near this line, giving the impression that it forms an approximate lower bound for their data. Because diffuse flow in the prism is primarily vertical, perpendicular to the sediment layers, the effective vertical permeabilities are probably controlled by the lower-permeability layers. The asterisk marks the harmonic mean of the permeability data plotted against the arithmetic mean of the porosities (excluding the anomalously low permeability value). Its location near lines h and m is consistent with the idea that the bulk permeability can be characterized in this fashion. For a discussion of the validity of extending this permeability porosity relation down to 10% porosity, the reader is referred to *Neuzil* [1994]. The final entry in the table was obtained with the permeability-void ratio relation of *Morin and Silva* [1984] and permits comparison of our model with that of *Screaton et al.* [1990]. The values in the table seem reasonable; however, the computed values of λ^* obtained for the back of the complex are below 0.1. These would be much too low to match the high pore pressures inferred from mud weights on Barbados Island [*Moore and Vrolijk*, 1992]. A second look at Figure 5 confirms that for porosities above 50%, such as exist near the toe, the permeabilities from this relation are reasonable, but at low porosities the values are unrealistically high.

Figure 8 is a plot of λ^* versus depth at an arcward distance of 20 km. The four curves represent different values for the décollement permeability when the bulk permeability is estimated using line m. As noted before, a value of $k_d = 10^{-15}$ m^2 gives unrealistically high values for λ^*. Higher values for k_d permit the décollement to act as a drain for the base of the complex. However, the rate of compaction at the base of the underthrust is sufficient to maintain modest overpressures even when $k_d = 10^{-12}$ m^2.

Table 1 also shows that none of the steady state concentrations approach the observed minimum value of 505 m*M*. A series of simulated concentration profiles obtained by varying k_d and the percent of bulk smectite are shown in Figures 9a and 9b, together with the measured data for ODP site 671. In all of the simulations, the prism and underthrust permeabilities

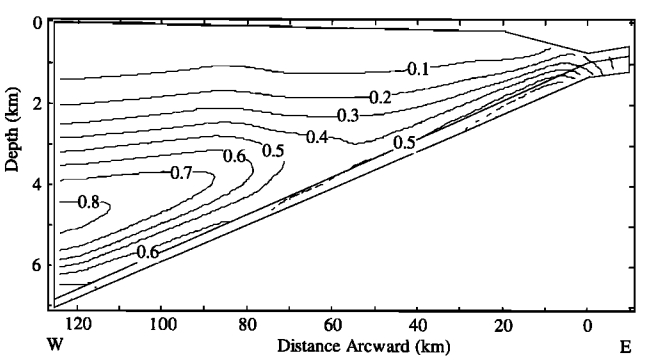

Figure 7. Contour plot of λ^* computed using the permeabilities in Figure 6 and $k_d = 10^{-14}$ m^2. Note that pore pressures are a significant fraction of lithostatic over the entire base of the complex.

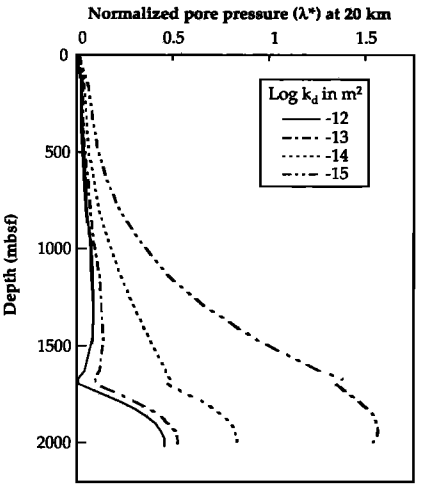

Figure 8. The effect of varying k_d on normalized pore pressures along a profile located 20 km arcward of the deformation front. The results indicate that the minimum possible k_d is between 10^{-14} and 10^{-15} m^2.

are those in Figure 6, the longitudinal dispersivity is 100 m, and the transverse dispersivity is 10 m. *McCaffrey* [1994] also varied the grid spacing and the dispersivity in the model. She found that with the above dispersivities, a horizontal node spacing near the toe of less than 100 m and a vertical node density of at least 30 rows (corresponding to dimensions of 20–150 m) gave results that were independent of the grid. The grid used in the present model satisfies this criterion, indicating that numerical dispersion is not appreciable. McCaffrey also found that using dispersivities less than $\alpha_L = 100$ m and $\alpha_T = 10$ m did not change the computed concentrations. Two features are clear from the plots. First, predicted concentrations along the décollement are too high, even when the percent of interlayer water released from the smectite is doubled. Second, the model predicts concentrations near the seafloor that are significantly lower than that of seawater.

The problem of low simulated concentrations at the seafloor may be due to an unreasonable assumption of a steady state transport model. Figure 10 shows a simulation in which the starting pore fluid concentration everywhere in the prism is that of seawater. The initial pressures correspond to a steady state flow solution with bulk permeabilities from Figure 6, $k_d = 10^{-13}$ m^2, and a bulk smectite content of 40%. The data from site 671 are also shown for comparison. The simulated profile at 1 m.y. does not have unreasonably low concentrations near the seafloor, but it also does not come anywhere near producing the 10% anomaly along the décollement. The emerging picture is that either there is another, unknown, source of fresh water or a constant value for k_d and steady state flow and transport do not accurately describe the system.

Transient Modeling Results

The possibility that the flow system is transient has been proposed by many authors [e.g., *Moore et al.*, 1988; *Karig*, 1990; *Bangs and Westbrook*, 1991; *Brown et al.*, 1994]. These authors cite observations of scaly fabrics in sediments along the décollement as evidence for a cyclic history of effective stress. The conceptual model is that the décollement sediments are first compacted as they are sheared and buried by the increasing depth of the overlying prism. The scaly fabrics indicate that at

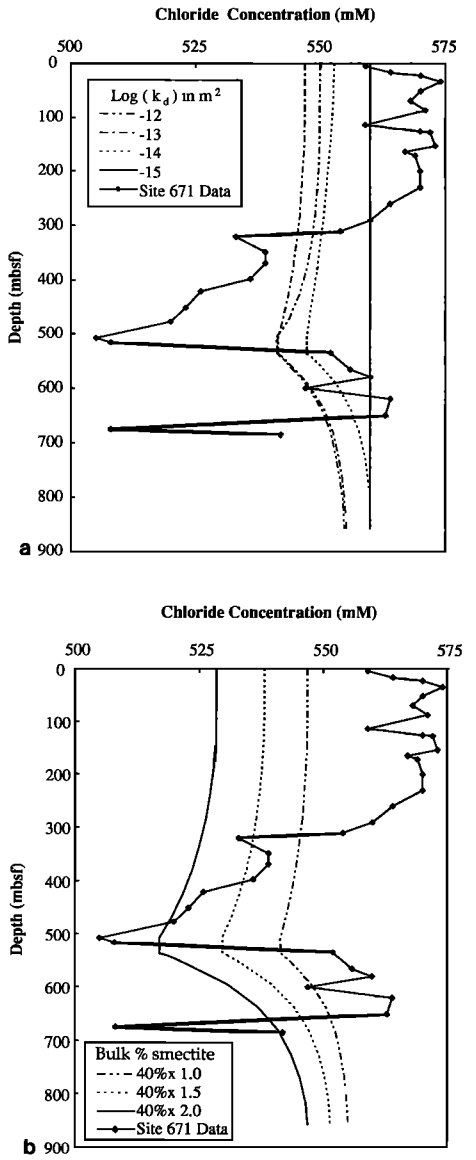

Figure 9. Simulated steady state chloride concentrations at site 671 obtained by (a) varying k_d with initial smectite equal to 40% and (b) varying the percent of smectite with $k_d = 10^{-13}$ m^2. All simulations give values that are too high along the décollement and too low at the seafloor.

some point the effective stress has dropped, probably because of an increase in pore pressures. If the bulk permeabilities in the complex are too low to drain the constant supply of fluids from compaction and dehydration of the underthrust sediments, then the pressures will build over time. Eventually, the pressure along the fault will lower the effective stress enough to overcome the frictional forces, and a period of slip will occur. During this period of slip, permeabilities along the fault may rise owing to hydrofracture or misalignment of asperities. The elevated pressures will then drive a transient flow system along the more permeable fault surface. This conceptual model leads to a cycle in which pressures build, are released, and then build again over time.

One of these cycles was simulated by setting the initial conditions to steady state pressures and concentrations corresponding to 40% smectite and $k_d = 10^{-14}$ m^2. At the start of the simulation, the fault permeability is increased instantaneously to 10^{-12} m^2, and the resulting flow and concentrations monitored at site 671. The simulated concentrations shown in Figure 11a are close to those of site 671 after 1000 years and reach minimum values within 10,000 years. The values near the seafloor are slightly lower than seawater, but this is caused by using a steady state solution for the initial condition. The décollement concentrations observed at ODP site 948 take about 4000 years to evolve. Note that the minimum value attained is almost 30% lower than the seawater value. *Buatier et al.* [1992] presented evidence that some smectite in the underthrust is transformed at low temperatures under high water/rock ratio conditions. This would result in a lower bulk percent of smectite in the sediments entering the reaction window. The results from Figure 9b indicate that the minimum concentration achieved along the décollement is proportional to the initial percentage of smectite. Thus the observed concentrations could still be achieved with as little as 26% smectite in the sediments entering the reaction window.

The pressures, shown in Figure 11b, rise dramatically along the fault during the first few thousand years, to slightly exceed lithostatic values. Thus, if it is possible for slip or hydrofracture to initially increase the fault permeability over a local area, the new flow system may then maintain the open fractures for several thousand years. These results support the concept of a cycle in which pressures build at depth until the lowered effective stress permits a strain event to occur. The strain opens fractures, resulting in greater permeability along the fault. The combination of high pressures and greater permeability leads to increased flow toward shallower depths. This, in turn, causes pressures at shallower depths along the fault to rise, providing a mechanism for keeping the fault open. In this scenario the increased flow comes from pore fluid that has been accumulating deep in the complex. This picture is consistent with recent seismic evidence that large patches of the décollement

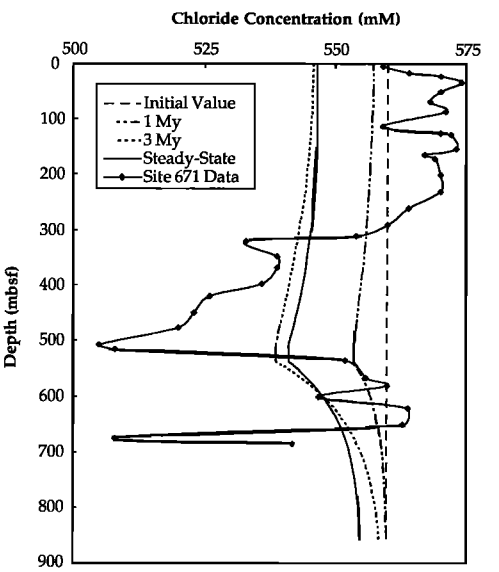

Figure 10. The results of a transient simulation with an initial chloride concentration equivalent to seawater, showing the rate at which the model approaches steady state. The result at 1 m.y. is probably more appropriate than the steady state solution, because the elapsed time since accretion at the location of site 671 is less than 1 m.y.

are dilated by near-lithostatic fluid pressures [*Bangs and Westbrook*, 1991; *Shipley et al.*, 1994].

A significant aspect of the transient pressures in Figure 11b is that they rise slightly higher than lithostatic values. Changing the value used for the aquifer compressibility, α, does not significantly alter this behavior. If this pressure increase actually occurs in nature, it will trigger some kind of release mechanism. One possibility is that the pulse could expand along the strike of the fault. Another is that it could escape along fractures in the overlying prism. This second possibility is supported by the low spikes in the chloride concentration data that correlate with major faults in the prism. In addition, the force balance analysis of *Davis et al.* [1983] predicts that the shape of the overlying prism must change in response to a drop in effective stress along the décollement. Thus, as the high–pore pressure pulse passes along the décollement, this change in shape might be accomplished by slip along the thrust faults in the overlying prism. A third possible pressure release mechanism is the formation of mud volcanoes, which have been observed at several locations in the complex.

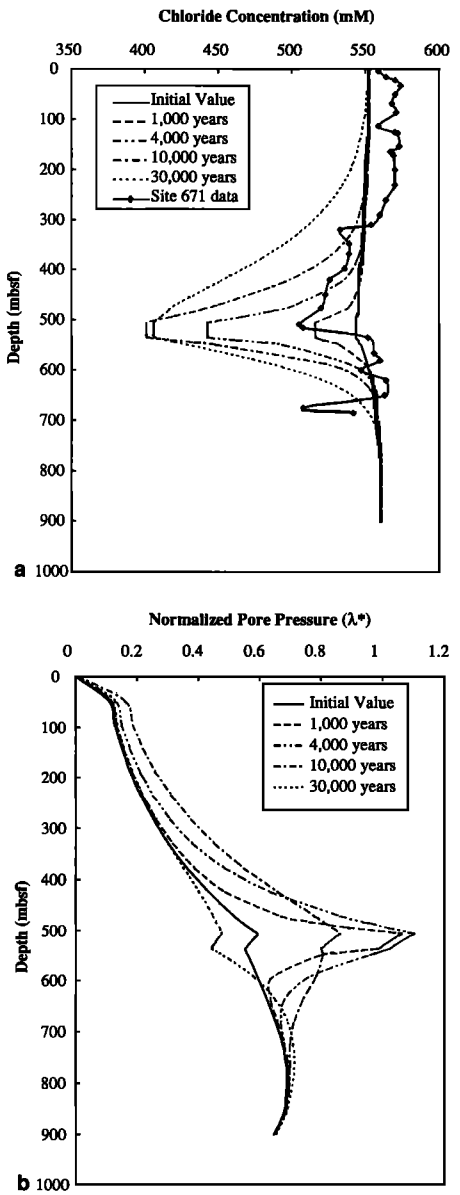

Figure 11. (a) Computed concentration and (b) normalized pore pressures at site 671 from a transient simulation in which k_d is increased along the 30 m décollement from 10^{-14} m^2 to 10^{-12} m^2 at the start of the simulation. Simulated concentrations are comparable to the data after 1000–4000 years. Normalized pore pressures along the fault increase with time, reaching lithostatic values within 1000 years.

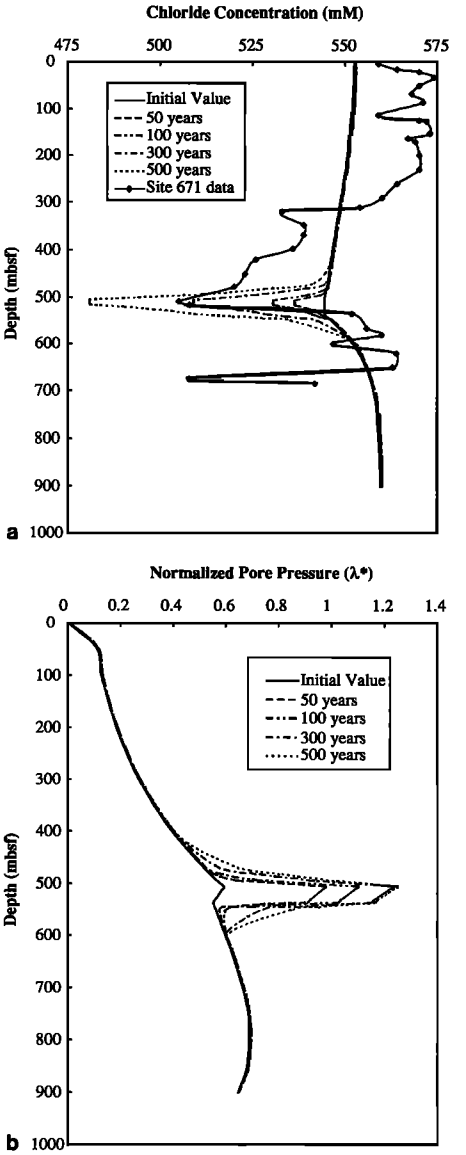

Figure 12. (a) Computed concentration and (b) normalized pore pressures at site 671 from a transient simulation in which k_d is increased over a 10-m-thick zone from 10^{-14} m^2 to 10^{-11} m^2 at the start of the simulation. Simulated concentrations are comparable to the data after 300 years. Normalized pore pressures along the décollement reach lithostatic values within 50 years.

In the transient scenario, there is a question regarding the thickness and lateral extent of the portion of the fault that is dilated. Figures 12a and 12b show the concentrations and pressures that evolve when permeability for a 10-m section of the fault (one third of the previous thickness) is increased to 10^{-11} m^2 and the prism permeabilities over the first 20 km are raised by 2 orders of magnitude. In this case, concentrations drop to the observed values in about 300–400 years, and pressures are

close to lithostatic in about 50 years. It is interesting to note that the times associated with the pressure and concentration profiles are proportional to k_d and inversely proportional to fault thickness. For example, in Figure 11, if the permeability of the open fault was 10^{-11} m^2 (instead of 10^{-12} m^2) then λ^* would reach 0.8 within 10 years (rather than 100 years). In addition, concentrations would drop to the observed values in 100–400 years, and pressures would remain elevated for at least 1000 years. The inverse relation to fault thickness implies that in Figure 12, if the fault thickness was 30 m instead of 10 m then concentrations close to those at site 671 would be achieved in 100 years.

For simplicity, the dilated portion of the fault in this model has encompassed the whole cross section. In reality, a limited patch of the fault will be dilated as slip propagates in an inchworm fashion. Thus these modeling results demonstrate that transience is a promising direction for further refinement of the model. The next generation of models will involve constitutive equations that describe the variation of k_d as fractures along parts of the décollement open and close in response to cycles of pore pressure.

Summary and Conclusions

We have created a two-dimensional cross-section model of the Barbados accretionary complex to test whether observed low-chloride pore waters could come from clay dehydration reactions at depth. The model simulates fluid flow and transport of total dissolved solids using a modified form of the program SUTRA [*Voss*, 1984]. The effects of sediment consolidation and fluid release by smectite dehydration are accounted for as source terms in the equations. The bulk permeabilities in the model must allow the source fluids to exit but also maintain observed pressures that are a significant fraction of lithostatic. The best fit permeabilities follow a porosity-permeability distribution centered within the outline compiled by *Neuzil* [1994]. The best fit décollement permeability was 10^{-14} m^2, which is the same as that obtained by *Screaton et al.* [1990] for a smaller model of the same location.

The model results indicate that a steady state flow system can account for the inferred pressure distribution but not for the observed chloride concentrations. Varying décollement permeabilities by 3 orders of magnitude and smectite percentages to twice the observed values fails to produce concentrations resembling the data. A transient scenario in which the fault permeability is suddenly raised 2–3 orders of magnitude is more promising. Simulated concentrations drop close to the observed values in 100–1000 years. In addition, pressures rise along the fault to near lithostatic in 10–100 years and remain elevated for 1000–10,000 years. The generation and persistence of elevated pressures in the transient model provide a mechanism for maintaining high pore pressures and permeabilities along the fault. This result may also explain the patches of high pore pressures along the décollement inferred from reversed polarity seismic reflections [*Bangs and Westbrook*, 1991; *Shipley et al.*, 1994]. Finally, it is consistent with the observed décollement sediment fabrics [*Karig*, 1990] and lab permeability test results [*Brown et al.*, 1994], suggesting that these sediments must be exposed to cycles of elevated pore pressures.

Acknowledgments. The funding for this work was provided by NSF grant OCE-9116462. We would also like to thank Chris Neuzil, Juli Morgan, Gretchen Zwart, and Steve Ingebritsen for careful and helpful reviews. Finally, the work has benefited greatly from discussions with Barbara Ransom, Kevin Brown, and Casey Moore.

References

Bangs, N. L. B., and G. K. Westbrook, Seismic modeling of the décollement zone at the base of the Barbados Ridge accretionary complex, *J. Geophys. Res.*, *96*, 3853–3866, 1991.

Bangs, N. L. B., G. K. Westbrook, J. W. Ladd, and P. Buhl, Seismic velocities from the Barbados Ridge complex: Indicators of high pore fluid pressures in an accretionary complex, *J. Geophys. Res.*, *95*, 8767–8782, 1990.

Bekins, B. A., and S. J. Dreiss, A simplified analysis of parameters controlling dewatering in accretionary prisms, *Earth Planet. Sci. Lett.*, *109*, 275–287, 1992.

Bekins, B. A., A. M. McCaffrey, and S. J. Dreiss, The influence of kinetics on the smectite to illite transition in the Barbados accretionary prism, *J. Geophys. Res.*, *99*, 18,147–18,158, 1994.

Bethke, C. M., Inverse hydrologic analysis of the distribution and origin of Gulf Coast–type geopressured zones, *J. Geophys. Res.*, *91*, 6535–6545, 1986.

Bouysse, P., D. Westercamp, and P. Andreieff, The Lesser Antilles Island Arc, in *Proc. Ocean Drill. Program Sci. Results*, *110*, 29–44, 1990.

Brown, K. M., The variation of hydraulic conductivity structure of an overpressured thrust zone with effective stress, *Proc. Ocean Drill. Program Initial Rep.*, in press, 1995.

Brown, K. M., B. A. Bekins, B. Clennell, D. Dewhurst, and G. Westbrook, Heterogeneous hydrofracture development and accretionary fault dynamics, *Geology*, *22*, 259–262, 1994.

Buatier, M. D., D. R. Peacor, and J. R. O'Neil, Smectite-illite transition in Barbados accretionary wedge sediments: TEM and AEM evidence for dissolution/crystallization at low temperature, *Clays Clay Miner.*, *40*, 65–80, 1992.

Capet, X., H. Chamley, C. Beck, and T. Holtzapffel, Clay mineralogy of ODP sites 671 and 672, Barbados Ridge accretionary complex and abyssal plain: Paleoenvironmental and diagenetic implications, in *Proc. Ocean Drill. Program Sci. Results*, *110*, 85–96, 1990.

Davis, D. M., J. Suppe, and F. A. Dahlen, Mechanics of fold and thrust belts and accretionary wedges, *J. Geophys. Res.*, *88*, 949–963, 1983.

Ferguson, I. J., G. K. Westbrook, M. G. Langseth, and G. P. Thomas, Heat flow and thermal models of the Barbados Ridge accretionary complex, *J. Geophys. Res.*, *98*, 4121–4142, 1993.

Fisher, A. T., and G. Zwart, Permeability and fluid pressure along the décollement of the Barbados accretionary complex: The first in-situ measurements, *Eos. Trans. AGU*, *75*, Fall Meet. suppl., 587, 1994.

Gieskes, J. M., P. Vrolijk, and G. Blanc, Hydrogeochemistry of the northern Barbados accretionary complex transect: Ocean Drilling Project leg 110, *J. Geophys. Res.*, *95*, 8809–8818, 1990.

Hawkins, R. K., and P. A. Egelstaff, Interfacial water structure in montmorillonite from neutron diffraction experiments, *Clays Clay Miner.*, *28*, 19–20, 1980.

Karig, D. E., Experimental and observational constraints on the mechanical behavior in the toes of accretionary prisms, in *Deformation Mechanisms, Rheology and Tectonics*, edited by R. J. Knipe and E. H. Rutter, *Geol. Soc. Spec. Publ. London*, *54*, 383–398, 1990.

Kastner, M., H. Elderfield, and J. B. Martin, Fluids in convergent margins: What do we know about their composition, origin, role in diagenesis and importance for oceanic chemical fluxes, *Philos. Trans. R. Soc. London, Ser. A*, *335*, 275–288, 1991.

Kastner, M., Y. Zheng, T. Laier, and P. Labaume, Origin, composition and flow of fluids in the fine-grained northern Barbados Ridge accretionary prism, *Eos. Trans. AGU*, *75*, Fall Meet. suppl., 587, 1994.

Kulm, L. D., et al., Oregon subduction zone: Venting, fauna, and carbonates, *Science*, *231*, 561–566, 1986.

Le Pichon, X., P. Henry, and S. Lallemant, Water flow in the Barbados accretionary complex, *J. Geophys. Res.*, *95*, 8945–8967, 1990.

Magee, M. E., and M. D. Zoback, Evidence for a weak interplate thrust fault along the northern Japan subduction zone and implications for the mechanics of thrust faulting and fluid expulsion, *Geology*, *21*, 809–812, 1993.

McCaffrey, A. M., The impact of the smectite to illite transformation on fluid flow and solute transport in the Barbados accretionary complex, M. S. thesis, Univ. of Calif., Santa Cruz, 1994.

Moore, J. C., and B. Biju-Duval, Tectonic synthesis, Deep Sea Drilling Project leg 78A: Structural evolution of offscraped and underthrust sediment, northern Barbados Ridge complex, in *Initial Rep. Deep Sea Drill. Proj.*, *78A*, 601–620, 1984.

Moore, J. C., and P. Vrolijk, Fluids in accretionary prisms, *Rev. Geophys.*, *30*, 113–135, 1992.

Moore, J. C., et al., Tectonics and hydrogeology of the northern Barbados Ridge: Results from Ocean Drilling Program leg 110, *Geol. Soc. Am. Bull.*, *100*, 1578–1593, 1988.

Morin, R., and A. J. Silva, The effects of high pressure and high temperature on some physical properties of ocean sediments, *J. Geophys. Res.*, *89*, 511–526, 1984.

Neuzil, C. E., How permeable are clays and shales?, *Water Resour. Res.*, *30*, 145–150, 1994.

Neuzil, C. E., Abnormal pressures as hydrodynamic phenomena, *Am. J. Sci.*, *295*, 745–789, 1995.

Peacock, S. M., Fluid processes in subduction zones, *Science*, *248*, 329–337, 1990.

Pytte, A. M., and R. C. Reynolds, The thermal transformation of smectite to illite, in *Thermal Histories of Sedimentary Basins*, edited by N. D. Naeser and T. H. McCulloh, pp. 133–140, Springer-Verlag, New York, 1988.

Ransom, B., and H. C. Helgeson, A chemical and thermodynamic model of aluminous dioctahedral 2:1 layer clay minerals in diagenetic processes: Regular solution representation of interlayer dehydration in smectite, *Am. J. Sci.*, *294*, 449–484, 1994.

Screaton, E. J., D. R. Wuthrich, and S. J. Dreiss, Permeabilities, fluid pressures, and flow rates in the Barbados Ridge complex, *J. Geophys. Res.*, *95*, 8997–9007, 1990.

Screaton, E. J., B. Carson, and G. P. Lennon, In situ permeability tests at ODP site 892: Characteristics of a hydrogeologically active fault zone on the Oregon accretionary prism, in *Proc. Ocean Drill. Program Init. Rep.*, in press, 1995.

Shipley, T. H., G. F. Moore, N. Bangs, J. C. Moore, and P. L. Stoffa, Seismically inferred dilatancy distribution, northern Barbados Ridge décollement: Implications for fluid migration and fault strength, *Geology*, *22*, 411–414, 1994.

Speed, R. C., and D. K. Larue, Barbados: Architecture and implications for accretion, *J. Geophys. Res.*, *87*, 3633–3643, 1982.

Suess, E., B. Carson, S. Ritger, J. C. Moore, M. Jones, L. D. Kulm, and G. Cochrane, Biological communities at vent sites along the subduction zones off Oregon, in *The Hydrothermal Vents of the Eastern Pacific: An Overview*, edited by M. L. Jones, *Bull. Biol. Soc. Wash.*, *6*, 475–484, 1985.

Taylor, E., and J. Leonard, Sediment consolidation and permeability at the Barbados forearc, in *Proc. Ocean Drill. Program Sci. Results*, *110*, 289–308, 1990.

Tribble, J. S., Clay diagenesis in the Barbados accretionary complex: Potential impact on hydrology and subduction dynamics, in *Proc. Ocean Drill. Program Sci. Results*, *110*, 97–110, 1990.

Voss, C. I., A finite element simulation model for saturated-unsaturated, fluid density–dependent groundwater flow with energy transport or chemically reactive single-species solute transport, *U.S. Geol. Surv. Water Resour. Invest.*, *84-4369*, 1984.

Vrolijk, P., A. Fisher, and J. Gieskes, Geochemical and geothermal evidence for fluid migration in the Barbados accretionary prism (ODP leg 110), *Geophys. Res. Lett.*, *18*, 947–950, 1991.

Westbrook, G. K., J. W. Ladd, P. Buhl, N. Bangs, and G. J. Tiley, Cross section of an accretionary wedge: Barbados Ridge complex, *Geology*, *16*, 631–635, 1988.

B. A. Bekins, U.S. Geological Survey, Mail Stop 496, 345 Middlefield Road, Menlo Park, CA 94025. (e-mail: babekins@usgs.gov)

A. M. McCaffrey, Earth Sciences Department, University of California, Santa Cruz, CA 95064.

(Received February 28, 1995; revised July 3, 1995;
accepted August 24, 1995.)